MOMENTUM SPREAD OF THE 200 MeV LINAC BEAM AT NAL

Shoroku Ohnuma

National Accelerator Laboratory

April 10, 1971

Summary

It is demonstrated by a simple calculation that the momentum spread of the 200 MeV beam from the linac at NAL can be reduced (or increased) by simply changing the rf phase between the last two cavities. The nonlinearity of the phase oscillation in the last cavity is utilized intentionally for this purpose. The lowest value obtainable in this scheme without using a buncher is $\Delta p/p = \pm 1 \times 10^{-3}$. This value is rather insensitive to the rf level of the last cavity ($\gtrsim 60\%$ of the design value) or to the beam intensity ($\lesssim 100$ mA). With a single buncher and a somewhat reduced rf level (90% of the design value with the synchronous phase changing from $-32°$ to $-20°$) in the first cavity, the momentum spread can be further reduced to $\Delta p/p = \pm 0.7 \times 10^{-3}$.

INTRODUCTION

The rf voltage per turn of the booster that is required for an efficient adiabatic trapping depends quadratically on the momentum spread of the injected beam,

$$V(\text{in kV}) \geq 7.7 \times 10^7 (\Delta p/p)^2; \quad \Delta p/p = \text{half width.}$$

Since the voltage program is based on a value of 100 kV at the injection,[1] the momentum spread of the injected beam must be $\pm 1 \times 10^{-3}$ or less. If one considers the inevitable increase of the momentum spread due to space charge forces[2] introduced in the transport between the linac and the booster (~50 m), the requirement for the output beam from the linac becomes more stringent. The usual practice is to use a debuncher which may turn out to be the only solution for achieving the design intensity in the booster. However, since installation of any debuncher is not planned for the initial operation, it is worthwhile to explore simple means of reducing the momentum spread of the linac output beam.

Momentum spread (or energy spread) in the linac beam is due to a finite acceptance area of the longitudinal (phase-energy) phase space around the synchronous point. If the phase oscillation is linear and the beam is perfectly "matched" to the (linearized) acceptance shape at the injection, the final momentum spread at 200 MeV will be,[3] in the adiabatic approximation,

$$\Delta p/p = \pm 0.4 \times 10^{-4} \text{ per } \pm 1^\circ \text{ initial phase spread.}$$

There are several effects which make the actual spread much
greater than this idealized value. Even with bunchers, it is
not possible to have a perfectly matched initial beam. Space
charge forces and drift spaces between two adjacent cavities
contribute to a growing mismatching. Phase motion is far from
linear and the filamentation in phase space due to nonlinearity
makes the "effective" area of the beam increase. The coupling
effect between transverse and longitudinal motion[4] is also
responsible for the deterioration of the beam quality. Fortu-
nately, all these effects are serious only at low energies and,
after 10-20 MeV, the mismatched beam simply rotates within the
acceptance area. A mismatched beam is characterized by a
"breathing" of the momentum spread (and the phase spread)[5] with
a large amplitude and, depending on the phase of this breathing
motion at the end of a linac, one can easily have a large momen-
tum spread. For example, initially unbunched beam (no energy
spread at .75 MeV) can have $\Delta p/p \simeq \pm 2.5 \times 10^{-3}$ at 200 MeV (NAL
linac, 20-40 mA).

A simple way to control the momentum spread at the end
of a multicavity linac is to shift the rf phase of the last
cavity relative to the incoming beam. The beam is in the
nonlinear region of the phase space and the spread of the
phase oscillation frequency in the beam is enhanced. One can
utilize this nonlinear characteristic to achieve a partial
debunching. For given cavity parameters, the amount of the

phase shift needed depends on the shape of the beam in the phase space at the entrance of that cavity.

PHASE-ENERGY OSCILLATION

Notation

W, ϕ : kinetic energy and phase of each particle

W_s, ϕ_s: synchronous energy and phase; design value of $\phi_s = -32^\circ$ in all cavities

λ : rf wave length = 1.4897 m

E_o : average acceleration field

T : transit time factor

$m_o c^2$: proton rest energy

$c\beta_s$, $m_o c^2 \gamma_s$, $m_o c \eta_s$: velocity, total energy and momentum of the synchronous particle

In the linear, adiabatic approximation, the phase and the energy of a particle along a linac (at a distance s) are

$$\Delta\phi \equiv \phi - \phi_s = \sqrt{\alpha S} \, \cos\left(\int_o^s \omega_\phi(s) \, ds + \theta_o\right)$$

$$\Delta W \equiv W - W_s = \sqrt{S/\alpha} \, \sin\left(\int_o^s \omega_\phi(s) \, ds + \theta_o\right) \quad (\theta_o = \text{const.})$$

The invariant phase space area in $(\Delta\phi) - (\Delta W)$ space is πS and the oscillation frequency ω_ϕ and the shape parameter α are

$$\omega_\phi(\equiv 2\pi/\lambda_\phi) = \sqrt{AB}, \qquad \alpha = \sqrt{A/B}$$

with

$$A = -(2\pi/\lambda)(m_o c^2 \eta_s^3)^{-1},$$

$$B = eE_o T \sin \phi_s.$$

The beam occupies an ellipse

$$\alpha^{-1}(\Delta\phi)^2 + \alpha(\Delta W)^2 = S.$$

The total number of phase oscillations, n_ϕ, in each cavity
($s = s_i$ to s_f) is then

$$n_\phi = \int_{si}^{sf} ds/\lambda_\phi(s).$$

Values of α, λ_ϕ and n_ϕ in each cavity are given in Table 1.

There are three effects which make the actual frequency
different from ω_ϕ. (1) Coupling with the transverse motion.
In the Langrangian which describes the motion of a particle
in a linac, the coupling effect is contained in terms of the
form

$$(r^2)^n (\Delta\phi)^m \qquad n, m = 1,2,\ldots$$

where $\underline{r}$ is the transverse coordinate of the particle. The
oscillation frequency is increased by a factor (lowest order)

$$1 + (1/2)(\pi r/\eta_s \lambda)^2.$$

The effect is not very important, a few percent at the injec-
tion and less than one-half percent after 10 MeV. (2) Space
charge forces.[6] In general, focusing action of the acceler-
ating field is weakened by space charge forces and the
oscillation frequency is 70%-80% of what is given in Table 1
when the beam intensity is of the order of 100 mA. Since
the longitudinal space charge force depends strongly on beam
sizes in all three directions, it is difficult to predict the
total number of phase oscillations without detailed numerical

calculations.   (3) <u>Nonlinearity</u>. The linear frequency ω_ϕ

applies only for a small amplitude oscillation. For a larger

amplitude $\left(|\Delta\phi| \lesssim |\phi_s|\right)$, the "instantaneous" frequency is

approximately given by

$$\omega_\phi\left[1 - (\Delta\phi)/(2|\tan(\phi_s)|)\right].$$

Thus the oscillation is slower $(\Delta\phi>0)$ or faster $(\Delta\phi<0)$ than

the linear one and a spiral is introduced in the beam shape.

If not corrected, this effect increases the final momentum

spread more than (1) or (2).

SIMPLIFIED TREATMENT AND RESULTS

There have been many studies made on the beam dynamics

in proton linacs, most of them quite elaborate requiring a

use of large digital computers. The purpose of the present

investigation is quite different from those. It was intended

to be something useful and practical in the control room of a

linac where there is a small digital computer for operating

the linac. For example, at NAL, such a computer has been used

not only for controlling the linac but also for obtaining the

beam emittance. The calculation presented here is therefore

based on the simplest possible approach. The transverse

motion is entirely omitted and the velocity dependence of the

transit time factor is ignored. For a high intensity beam,

the calculation starts at a point where space charge effects

are expected to be negligible. This means a certain beam

shape in the phase space is assumed at the end of the second
or the third cavity as something beyond the control and the
method is applied after that.

From the drift tube table of the linac, a simple inter-
polation formula is derived for the synchronous velocity in
each cavity. The velocity is assumed to change abruptly at
the center of each cell. Energy gain of the synchronous
particle is then calculated and this is multiplied by
$\cos(\phi)/\cos(\phi_s)$ to find the energy gain for a nonsynchronous
particle. The phase change from one gap to the next is
simply

$$\delta(\Delta\phi) = (2\pi)(\beta_s - \beta)/\beta$$

since velocities β_s and β are assumed to be constant between
the two gaps. Similarly, the effect of a drift space (length
d) between two cavities is

$$\delta(\Delta\phi) = -(2\pi d/\lambda)(\Delta W/m_o c^2 \eta_s^3).$$

With a minor change, the calculation is extended to cases in
which the rf level is less than 85% of the design value so
that there is no real synchronous phase (no stable area). The
beam can be placed anywhere in the phase space by simply shift-
ing the rf phase of a cavity relative to the previous one.
However, a caution is required when β is much less than β_s.
Phase of the accelerating field changes appreciably within a
single gap for such a particle and the transit time factor
becomes meaningless in the calculation of the energy gain.

Indeed, even very elaborate calculations reported previously
are not much reliable for investigating the behavior of "lost"
particles.

Because of the phase damping ($\beta^{-1/2} \sim \beta^{-3/4}$, depending on
the amount of space charge effects), the phase motion is
approximately linear after the first cavity (10.4 MeV) and
the essential features of the nonlinearity can be seen at the
end of the first cavity. Two curves are given in Fig. 1; the
solid curve is for a "d.c." beam at the injection (750 keV)
and the dashed curve for a bunched beam, both at the end of
the first cavity. The buncher voltage is 22.5 kV and its
distance to the linac is 88.7 cm. Relative phases $\Delta\phi$ at the
first gap (for the solid curve) or at the buncher (for the
dashed curve) are also shown along these curves. Phase
acceptances are $\Delta\phi = -41.4°$ to $64°$ (28%) and $\Delta\phi = -114.6°$ to
$132.1°$ (69%), respectively. It is seen that the tails of
these two curves are almost identical so that, if one considers
the entire beam, there will be no difference in the final
momentum spread. It is, of course, advantageous to use a
bunched beam since, in practice, one is interested in the
momentum spread of, say, 95% of the beam. Under the normal
condition, that is, if the beam is placed around the synchro-
nous point in each cavity, its shape at the end of the linac
is quite unfavorable as far as the momentum spread is con-
cerned. This can be seen in Fig. 2 where the solid curve is

at the end of the linac (cavity No. 9) and the dashed curve

is at the end of the cavity No. 8. Since the number of phase

oscillations is close to one-quarter (see Table 1), the large

phase spread (~15°) of the dashed curve is converted to the

large momentum spread of the solid curve. If the beam is

shifted to the right, the oscillation frequency is smaller

for particles on the right (large, positive $\Delta\phi$) than on the

left because of the nonlinearity. At the same time the number

of oscillations becomes less than one quarter for the entire

beam and the bunch may move in the phase space without rotat-

ing around its own center. On the other hand, if it is

shifted too much to the right, part of the beam moves along

"unstable" flow lines causing a large momentum spread. The

oscillation frequency can also be controlled by changing the

rf level in the last cavity. The dependence of the frequency

on the accelerating field E is

$$\omega_\phi^2 \propto \sqrt{E^2 - E_o^2 \cos^2\phi_s}; \quad E_o, \; \phi_s = \text{design value}$$

with the synchronous phase

$$\phi_s' = \cos^{-1}(E_o \cos \phi_s / E).$$

Expected values of momentum spread are shown in Fig. 3 under

different operating conditions of the last cavity. Central

energy of the beam at the optimum point is different for

different values of ϕ_s' as indicated in the figure. However,

the optimum value of $\Delta p/p(\pm0.8\sim\pm1.0\times10^{-3})$ is rather insensi-

tive to the rf level and, although not shown here, the rf

level can be as low as ~60% of the design value. Note that

below 85%, there is no synchronous phase and the motion is

entirely "unstable." The expected shape of the momentum

spectrum when $E = E_0$ and the amount of beam shift = 37.5°

is shown in Fig. 4. A beam size of ±1.5 mm (which corres-

ponds to $\Delta p/p = \pm 0.5 \times 10^{-3}$) at the focal plane of an analyz-

ing magnet is assumed in order to make a direct comparison

with the measurement made by the linac group. The dashed

curve in Fig. 4 is the result of a computer run[*] using the

program PARMILA.[7] Effects of transverse motions are included

in the calculation with the invariant transverse beam quality

of 1.0 π mm-mrad. In general, transverse motion affects the

final momentum spread only slightly (≲5%).

The scheme discussed here is applicable even when space

charge effects are important. A computer program developed

at Los Alamos, SCHEFF I,[8] has been used to find the beam

shape at the end of cavity No. 8 for high intensity beams.

When the intensity is 75 mA (design value of the NAL linac)

and other parameters are identical to low intensity beams

discussed above, 96% of the beam is contained within an

ellipse

$$\gamma (\Delta\phi)^2 + 2\alpha (\Delta\phi)(\Delta W) + \beta (\Delta W)^2 = A$$

---

with

$$\alpha = 0.120 \text{ MeV/degree}, \quad \alpha = 0.882,$$

$$\beta = 14.82 \text{ degree/MeV and } A = 4.32 \text{ degree-MeV.}$$

Because of the space charge effect on the oscillation fre-
quency, the orientation of the beam is different from the
one shown in Fig. 2. Thirty points along the boundary of
this ellipse have been traced in the last cavity using the
simple procedure (no transverse motion, no space charge).
Effects of shifting the beam relative to the rf phase in
the cavity are shown in Fig. 5. It is interesting to see
that again the optimum value, $\Delta p/p \simeq 1 \times 10^{-3}$, is insensitive
to the rf level. Results of the simple calculation given in
Fig. 5 are generally in good agreement with SCHEFF runs that
are continued to the end of the linac. Figs. 6-8 are typical
examples of SCHEFF runs with $E = E_o(\phi_s' = -32^\circ)$. One can see
in Fig. 8 that the shift of 35° causes the right side of the
beam to move down along unstable flow lines. The momentum
spread will increase rapidly as the amount of shift is
increased beyond this.

DISCUSSION

It is conceivable to design a multicavity linac taking
into account a definite shape of the output beam. However,
the shape is strongly dependent on other parameters (rf level,
intercavity phase and the beam intensity) and a linac so

designed will be quite inflexible. Shifting of the beam
relative to the rf phase of the last cavity seems to be the
simplest way to control the momentum spread.

There are other possibilities of reducing the momentum
spread which are somewhat more difficult. (1) Smaller
synchronous phase angle in the first cavity. It is clear
from Fig. 1 that, with or without a buncher, the tail part
of the beam in the phase space makes a sizable contribution
to the final momentum spread. A smaller synchronous phase
$(|\phi_s'| < 32^\circ, E < E_o)$ in the first cavity effectively rejects
this part. However, since the lowest-order nonlinear term
in the equation of phase oscillation is proportional to
$(\Delta\phi)/\tan|\phi_s'|$, the distortion due to nonlinearity is not
reduced. With $\phi_s' = -20^\circ$, the fraction of the bunched beam
captured in the first cavity is 62% compared to 69% for -32°
so that the reduction in the beam intensity is 10%. If the
beam is shifted properly in the last cavity, the final momen-
tum spread becomes as small as $\pm0.6 \times 10^{-3} (\phi_s' = -40^\circ)$
$\sim \pm0.7 \times 10^{-3} (\phi_s' = -32^\circ)$. One disadvantage of this scheme
is the more stringent requirements on the rf level of the
first cavity as well as on the relative phase between the
buncher and the linac. For example, a drop of 5% in the rf
level causes the synchronous phase to change from -32° to
-27°, which is not too serious, but from -20° to -8° that
will be disastrous. (2) Controlling the total number of

phase oscillation by changing the synchronous phase. The
dependence of the oscillation frequency ω_ϕ on the synchronous
phase ϕ_s' is

$$\omega_\phi \propto \sqrt{E \sin|\phi_s'|} = \sqrt{E \cos \phi_s'} \sqrt{\tan|\phi_s'|}$$

where $(E \cos \phi_s')$ is a constant machine parameter. By raising
or lowering rf levels in cavities, one can change the synchro-
nous phase and therefore the total number of oscillations
such that the beam comes out of the linac with a small momen-
tum spread. Two examples are seen in Fig. 9, both for an
initially unbunched beam. If ω_ϕ is to be increased substan-
tially in a single cavity, the required increase in the rf
level may not be realizable due to a limit in the available
rf power. Also, the transverse defocusing action of the
accelerating field (proportional to $\sin|\phi_s'|$) will be increased.
On the other hand, a drastic reduction in ω_ϕ in one cavity
requires a very small value of $|\phi_s'|$ and consequently a <u>linear</u>
phase space area that may be too small to contain the beam.
An adjustment involving 3~4 cavities seems unavoidable.

(3) <u>Debunching of the beam around the unstable fixed point</u>

<u>($\phi = -\phi_s$)</u>. Around the unstable fixed point, $\phi = -\phi_s$, the
linear phase oscillation is represented by hyperbolas

$$\alpha^{-1}(\Delta\phi)^2 - \alpha(\Delta W)^2 = \text{constant}/\alpha, \quad \alpha = \sqrt{|A/B|}.$$

The magnitude of $(\Delta\phi)$ and ΔW grows exponentially,

$$(\Delta\phi), \quad (\Delta W) \sim \exp(\sqrt{|AB|}s).$$

A way to debunch high energy beams based on this has been
discussed by L. Teng.[9] Although the emphasis is placed only
on stretching the beam, the scheme may be useful for reducing
the momentum spread as well. The beam is placed around the
unstable point in the next to the last cavity. At the end of
the cavity, the total phase spread of the beam is large, 50°
for $\phi_s' = -32^\circ$ and 32° for $\phi_s' = -12^\circ$. Two parameters, the
amount of beam shift and the rf level in the last cavity, are
then adjusted to make the final momentum spread as small as
possible. Unfortunately, the last cavity of the NAL linac
is too "long" for this scheme. The momentum spread is much
larger than $\pm 1 \times 10^{-3}$ either due to an excessive amount of
the beam rotation in $(\Delta\phi)-(\Delta W)$ space (when $E > E_o$, $|\phi_s'| > 32^\circ$)
or due to a large nonlinear distortion of the beam (when
$E < E_o$, $|\phi_s'| < 32^\circ$). If the last cavity were one-third of the
actual length, this method would be ideal. Nevertheless, if
space charge effects on the momentum spread are serious in
the subsequent transport system, it may turn out to be the
most favorable one because of the large beam size in the lon-
gitudinal direction. It should be remembered that the ulti-
mate object is to have a small momentum spread in the beam
injected into the booster but not necessarily in the beam at
the end of the linac.

The dependence of the momentum spread on the relative
phase between the last two cavities has been confirmed by
many measurements at NAL. When all cavities are properly

adjusted, the best value is $\Delta p/p = \pm 0.7 \times 10^{-3} \sim \pm 1.0 \times 10^{-3}$ at 20 mA. Uncertainties are mostly due to the beam size correction and a small background correction.

REFERENCES

1. Design Report ("White Book"), National Accelerator Laboratory, July 1968, p. 9-26.

2. L. Smith, NAL Report FN-146, May 9, 1968.

3. Parameters for the NAL linac are given in C. D. Curtis et al., Particle Accelerator 1 (1970), 93.

4. R. L. Gluckstern, Proceedings of the 1966 Linear Accelerator Conference, Los Alamos Scientific Laboratory, p. 207; S. Ohnuma, ibid., p. 214.

5. S. Ohnuma, Yale Report Y-17, January 19, 1967.

6. R. L. Gluckstern, Linear Accelerators (edited by P. M. Lapostolle and A. L. Septier, North Holland, 1970), p. 827.

7. D. A. Swenson and J. E. Stovall, LASL Report No. MP-3-90 (1969).

8. J. E. Stovall, LASL Report MP-3-19 (1968).

9. L. C. Teng, Minutes of the Conference on Proton Linear Accelerators, Yale University, October 21-25, 1963, p. 49.

Table 1

CHARACTERISTIC PARAMETERS OF THE LINEAR
PHASE OSCILLATION IN THE NAL LINAC

Cavity	Cell	Energy (MeV)	$\alpha\,(\text{MeV}^{-1})$	λ_ϕ (m)
1	1	.78	10.80	1.019
	29	3.66	2.906	2.806
	56	10.25	1.189	5.411
		number of linear oscillations = 2.68		
2	1	10.58	1.201	5.737
	31	22.41	.6858	10.19
	60	37.26	.4787	15.42
		number of linear oscillations = 1.91		
3	1	37.91	.4091	13.53
	18	51.28	.3318	17.45
	35	65.74	.2807	21.67
		number of linear oscillations = 0.953		
4	1	66.62	.2782	21.92
	29	92.09	.2254	29.44
		number of linear oscillations = 0.654		
5	1	93.04	.2181	28.95
	24	116.0	.1894	35.63
		number of linear oscillations = 0.484		
6	1	117.0	.1883	35.92
	22	138.5	.1696	42.30
		number of linear oscillations = 0.398		
7	1	139.5	.1687	42.57
	21	160.0	.1552	48.85
		number of linear oscillations = 0.347		
8	1	161.0	.1545	49.16
	20	180.5	.1444	55.28
		number of linear oscillations = 0.304		
9	1	181.5	.1438	55.55
	19	199.8	.1361	61.52
		number of linear oscillations = 0.269		

Total number of linear oscillations = 8.0

Fig. 1 Beam at the end of cavity No. 1
Solid curve: unbunched
                 acceptance $-41.4° \sim 64°$

Dashed curve: bunched
                 acceptance $-114.6° \sim 132.1°$

$\Delta W(MeV)$

$\Delta\phi$ (degrees)

ΔW(MeV)

$\Delta p/p(10^{-3}) = 2.7 \, \Delta W$ for solid curve

$= 3.0 \, \Delta W$ for dashed curve

Fig. 2

Solid curve: end of cavity No. 9

Dashed curve: end of cavity No. 8

Synchronous phase $= -32^{\circ}$
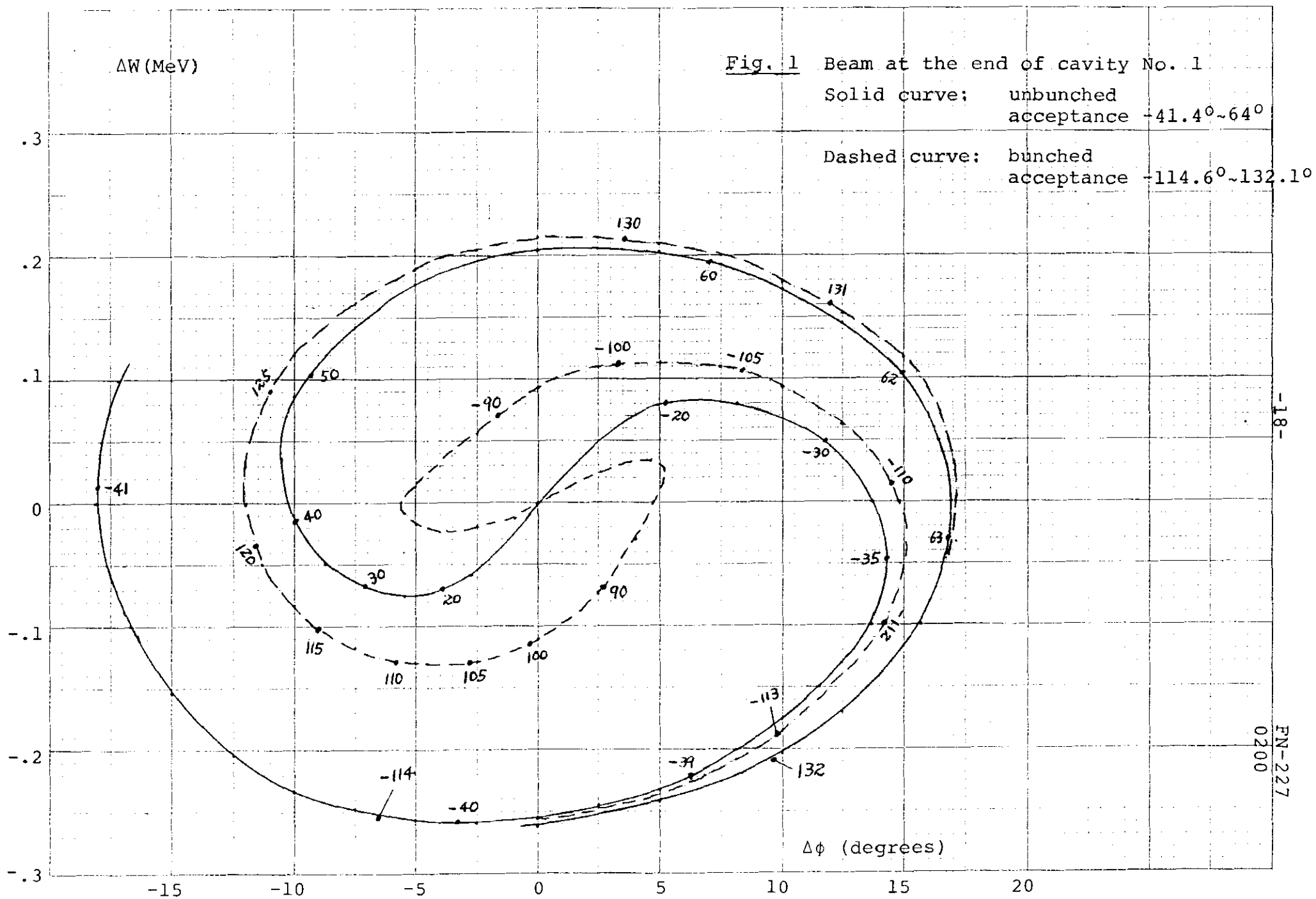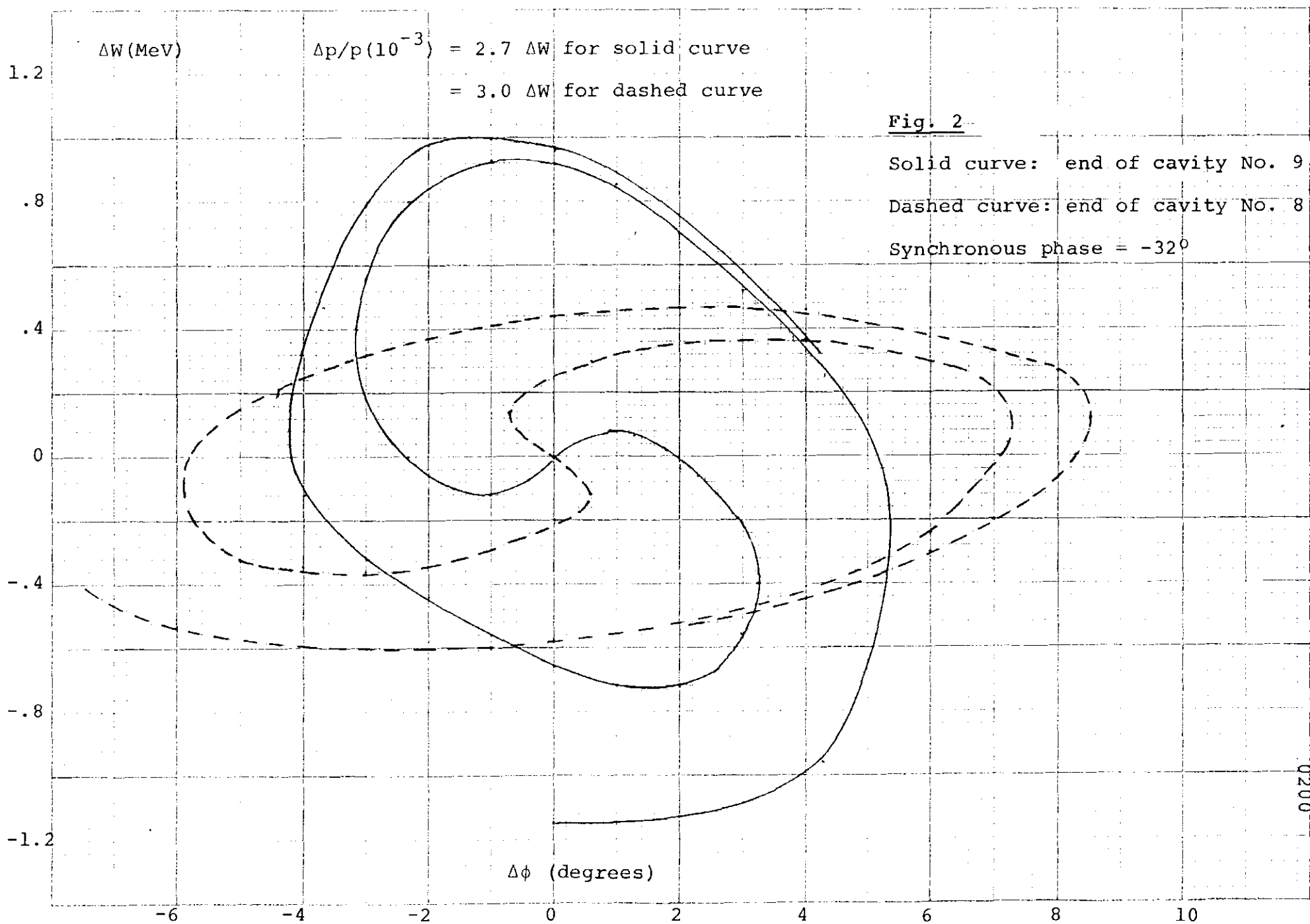
$\Delta\phi$ (degrees)

Δp/p (full width)   94% of the beam within Δp/p

4×10^{-3}

3

(1)   (2)   (3)

2

(4)

(5)

Fig. 3

	(1)	(2)	(3)	(4)	(5)
E/E_o	.85	.86	.90	1.00	1.11
ϕ'_s	0	-10	-20	-32	-40
W_c (MeV)	200.3	200.6	201.5	203.6	205.7

W_c = central energy of the beam at the minimum Δp/p

1

Phase shift (degrees)

0 -10   0   10   20   30   40   50   60

Arbitrary Scale

MOMENTUM SPECTRUM

Fig. 4 | Energy = 203.6 MeV for $\Delta p/p = 0$.

$\phi_s = -32°$, Phase shift = $+37.5°$

Solid curve: Simple method
Dashed curve: PARMILA

Beam size correction included

$\Delta p/p$ (in 10^{-3})

Fig. 5 Momentum spread as a function of rf level and phase shift in the last cavity.

Beam Current 75 mA

OUTPUT AT END OF CELL NO.286

Fig. 6   SCHEFF I $\Delta W = W-200.2$ MeV ΔW(MeV)

Initially unbunched beam
500 particles
$\phi_s = -32°$ (All cavities)

No phase shift

$\Delta\phi$ (degrees)

-12   -8   -4   4   8   12   16

ORDINATE DE   ABSCISSA DPHI
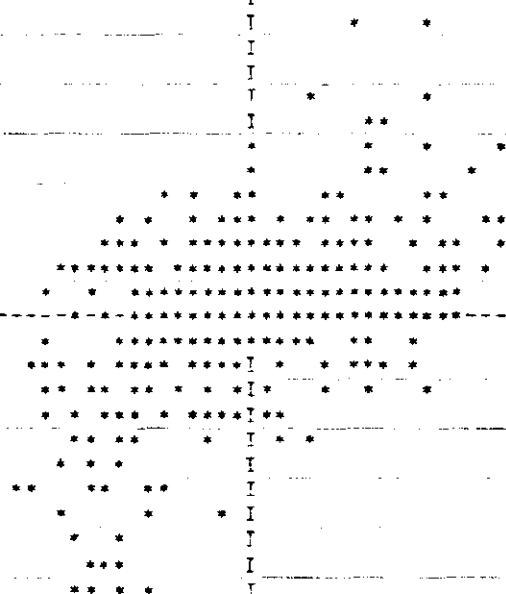
-23-

FN-227
0200

END OF RUN

OUTPUT AT END OF CELL NO.286   I= 20.0000

Fig. 7   SCHEFF I $\Delta W = W-203.2$ MeV ΔW(MeV)

Initially unbunched beam
500 particles
$\phi_s = -32°$ (All cavities)

Phase shift = $+30°$

$\Delta\phi$ (degrees)

-12   -8   -4   4   8   12   16

I= 20.0000

ORDINATE DE   ABSCISSA DPHI

END OF RUN

Fig. 8   SCHEFF I

Initially unbunched beam
500 particles
$\phi_s = -32°$ (All cavities)

Phase Shift = $+35°$

$\Delta W = W-203.4$ MeV

Fig. 9

		Cavity	
(1) ϕ_s =	$-32°$	No. 1 – No. 6	
	$-20°$	No. 7 – No. 9	
(2) ϕ_s =	$-32°$	No. 1 – No. 2	
	$-20°$	No. 3 – No. 5	
	$-15°$	No. 6 – No. 7	
	$-10°$	No. 8 – No. 9	

$\Delta p/p \ (10^{-3}) = 2.7 \ \Delta W (MeV)$

$\Delta W (MeV)$

$\Delta \phi$ (degrees)